Acta Materialia 174 (2019) 16–28

Contents lists available at ScienceDirect

Acta Materialia

journal homepage: www.elsevier.com/locate/actamat

Full length article

Large scale 3-dimensional atomistic simulations of screw dislocations interacting with coherent twin boundaries in Al, Cu and Ni under uniaxial and multiaxial loading conditions

Maxime Dupraz [a], Satish I. Rao [b, c], Helena Van Swygenhoven [a, d, *]

[a] Photons for Engineering and Manufacturing, Paul Scherrer Institut, 5232 Villigen PSI, Switzerland
[b] Materials Directorate, Air Force Research Laboratory, WPAFB, OH 45433, USA
[c] UES Inc., Beavercreek, OH 45432, USA
[d] Neutrons and X-Rays for Mechanics of Materials, École Polytechnique Fédérale de Lausanne, 1015 Lausanne, Switzerland

ARTICLE INFO

Article history:
Received 12 December 2018
Received in revised form
10 May 2019
Accepted 11 May 2019
Available online 15 May 2019

Keywords:
Molecular dynamics
Twin boundary
Screw dislocation
Face-centered cubic crystals
Multiaxial loading

ABSTRACT

Large scale 3D atomistic simulations are performed to study the interaction between a curved dislocation with a dominant screw character and a Coherent Twin Boundary (CTB). Three FCC metals (Al, Cu and Ni) are addressed using 6 embedded-atom method (EAM) potentials. The reaction mechanisms are studied first under uniaxial stress showing that transmission mechanism and critical transmission stress depend on the material considered and differ from results reported in quasi- 2D simulations. Then, the influence of multiaxial stresses including shear components in the CTB is investigated. It is shown that the influence of the loading conditions, which can be represented in terms of the Escaig stress, is material dependent. In Al and Cu, the critical transmission stress is largely dependent on the Escaig stress while only mildly for Ni. The presence of a shear component in the CTB tends to increase the critical transmission stress for all three materials. The absorption and desorption mechanisms of the screw dislocation are correlated with a potential energy barrier.

1. Introduction

The interaction of dislocations with a coherent twin boundary (CTB) of type $\sum 3\{1\,1\,1\}\langle 1\,1\,0\rangle$ has been extensively studied since the early observations of twinning in face centered cubic (FCC) metals [1]. The demonstration that the toughness of a polycrystalline FCC metal can be increased when grains contain a very high density of grown-in twins [2,3] suggest that the CTB act as a barrier for dislocation slip but that under certain conditions slip can be transferred across the CTB. In a search to understand the details of the interaction mechanism, dedicated experiments [4–7] and an extensive set of atomistic simulations have been performed [8–19]. It has been established that the mechanism for slip transfer is not the same for all FCC metals, that CTBs do not act as effective barrier for all crystal orientations [20] and that mechanism and values for barrier strength depend to a large extent on the interaction potential and the simulation geometry applied in the atomistic simulations [7]. However, there is no comprehensive analytical model that describes the role of twin densities in constitutive equations required for mesoscopic polycrystal plasticity models.

Why are there still so many open questions? In a FCC metal, a dislocation with Burgers vector $\boldsymbol{b} = \frac{a}{2}\left[1\,1\bar{}\,0\right]$, where a is the lattice parameter, gliding on a $(1\,1\,1)$ plane will dissociate into two Shockley partial dislocations $\frac{a}{6}[1\,\bar{2}\,1]$ and $\frac{a}{6}[2\,\bar{1}\,\bar{1}]$, because this lowers the total elastic energy [21]. These partial dislocations are bound by a stacking fault which in the absence of stress has an equilibrium distance determined by the stacking fault energy (SFE) and the elastic constants of the material [21]. When a screw dislocation impinges on a CTB under the influence of stress, different interaction mechanisms have been observed: the leading and trailing partial can be sequentially transmitted into the twinned grain by the so-called Fleischer (FL) [22,23] mechanism [14], alternatively leading and trailing can constrict into a perfect dislocation and get transmitted into the twinned grain by the Friedel-Escaig (FE) [24,25] mechanism [7,8,19]. Using the same FE

* Corresponding author. Photons for Engineering and Manufacturing, Paul Scherrer Institut, 5232 Villigen PSI, Switzerland.
E-mail address: helena.vs@psi.ch (H. Van Swygenhoven).

https://doi.org/10.1016/j.actamat.2019.05.025

mechanism, the incoming dislocation can also be absorbed in the CTB plane rather than being transmitted into the twinned region, with the two partials gliding along opposite directions without being bound by the stacking fault [7,8,12]. The process that controls the reaction mechanism is still subject to debate [7,8]. Several material parameters play a role in whether a dislocation gets absorbed or transmitted and how transmission occurs. There is for instance the role of the SF making it easier or more difficult to constrict the dislocation and the effect of the Escaig stress, *i.e.* the component of the shear stress within the slip plane acting on the edge component of the Shockley partials and causing constriction or separation of the latter depending on its sign. There are other material differences that are less well understood. For instance the interaction of a dislocation is systematically repulsive when the dislocation is far from the CTB, but at closer distances becomes attractive in Al leading to spontaneous absorption of the dislocation [11] however remains repulsive in Ni and Cu [11,12]. Using quasi 2D simulation geometries with periodic boundary conditions along the dislocation line, it is mostly observed that in Al the dislocation remains absorbed in the CTB whereas in Cu and Ni the dislocation can transmit via the FE mechanism [7,8]. The transmission stresses are usually high and depend on the interatomic potential used. In quasi 2D simulations, due to the periodic boundary conditions, the dislocation is always straight when impinging on the CTB, its length is defined by the size of the simulation box and the constriction of the stacking fault has to occur over the entire length. Concurrent atomistic-continuum simulations (CAC) [19] used to study the sequential slip transfer of a series of curved dislocations from a pile-up on a $\sum 3$ CTB in Cu and Al, suggested the importance of the dislocation line curvature and dislocation length in the interaction mechanism and transmission stress. Furthermore, the mechanisms derived from quasi 2D simulations are obtained mostly by applying uniaxial tensile stress along the CTB. In reality, the CTB inside a grain in a polycrystalline grain boundary network will experience non uniaxial stresses as well as stress conditions including shear components acting in the CTB [26].

In this paper we simulate the screw dislocation/CTB interaction using a 3D modeling approach exploring more realistic dislocation configurations. The reaction mechanisms are studied for Al, Ni and Cu using different EAM potentials first under uniaxial tensile stress allowing comparison with quasi 2D simulations. Then the influence of multiaxial stresses including shear components in the CTB is investigated and the results are discussed in terms of potential energy barrier.

2. Methods

2.1. Potentials

Al, Cu and Ni are modeled with different EAM potentials: for Al the potentials developed by Mishin et al. [27] (Al99), Zope and Mishin [28] (Al03) and Liu and Ercolessi [29] (Al-LEA), for Cu by Mishin et al. [30](Cu01) and Mendelev et al. [31] (Cu12) and for Ni by Mishin et al. [27] (Ni99). Several interatomic potentials are considered for Al and Cu, in order to evaluate the influence of the potential on the interaction mechanism and/or the critical transmission stress and strengthen the trends presented in section 3. Indeed, as evidenced by Chassagne *et al.* [7] the critical transmission stress may strongly depends on the selection of the interatomic potential. The material parameters for these potentials are listed in Table 1: where b_p is the magnitude of the Shockley partial Burgers vector, μ the $\{1\,1\,1\}<1\,\bar{1}\,0>$ shear modulus, γ_S the intrinsic SFE, γ_T the twin energy, *i.e.* the CTB surface energy, γ_{US} the unstable SFE and γ_{UT} the unstable twin energy. Due to the fact that the SFE is generally not included in the list of fitted parameters, this quantity is often underestimated in the EAM formalism. This is not the case for the potentials selected, which predict SFEs in relative good agreement with experiment.

2.2. Simulation cell

Fig. 1 shows the simulation cell used to simulate the interaction of a curved dislocation with dominant screw character with the CTB. Free surfaces are used as boundary conditions in all three directions of space. To understand the geometry of the bi-pillar, it is convenient to use a Thompson tetrahedron that is mirrored across the $(1\,1\,1)(\delta)$ plane (supplementary material A).

This common mirror plane represents the twin boundary. The lattice orientations corresponding with the axes of the simulation cell are X[1 1 1], Y[$\bar{2}$ 1 1], Z[0 $\bar{1}$ 1] and X′[1 1 1] $_T$, Y′[2 $\bar{1}$ $\bar{1}$]$_T$, Z′[0 1 $\bar{1}$]$_T$ for the incoming and outgoing (twinned) grains respectively. This simulation cell mimics the bi-pillar geometry used for compression experiments in Ref. [4]. In directions X, Y and Z the cell lengths are $Lx = 108a\sqrt{3}$, $Ly = 40a\sqrt{6}$ and $Lz = 70a\sqrt{2}$, corresponding to approximately 7.2 million atoms. The simulation cell size of the three materials differs only by the lattice parameter. For Al with a = 4.05 Å, the dimensions of the bi-pillar are 745x395x405 Å^3 which is between one and two orders of magnitude smaller than the typical size of pillars that are used in compression experiments. Simulations were also performed on a bi-pillar with varying size along the Y and Z directions, allowing evaluation of the influence of the image forces due to the presence of the free surfaces [11] and their effect on the reaction mechanism and the critical stress for transmission (σ_{rss_trans}). Note that the image forces/size effects have been evaluated for only one stress state (uniaxial z-tension). Indeed as discussed in supplementary material B, a systematic evaluation of the image forces for each multiaxial stress state would have required too much computing time. Varying the size of a simulation cell under z-tension has no influence on the interaction mechanism and does not dramatically affect σ_{rss_trans} for the material/potential considered.

In Al and Cu, while doubling the length along Z does not produce any measurable effect, increasing the dimensions along Y tends to slightly decrease the value of σ_{rss_trans} (Table B1). This suggests that the length of dislocation line that interacts with the CTB is one of the parameters that control the value of the transmission stress. Considering the computational cost, all the simulations presented in this work are performed on the reference cell *Lx*, *Ly*, *Lz*. As illustrated in Fig. A1 only three Burgers vector are shared by both grains, *i.e.* lie on the common (1 1 1) mirror plane: these dislocations can glide on one slip plane in each grain. By definition, these dislocations will always have the highest Schmid factor when the twin boundary is parallel to the loading/compression axis as shown by Li et al. [15].

After an initial relaxation of the system with energy minimization, a perfect screw dislocation with $\boldsymbol{b} = \frac{a}{2}[1\,\bar{1}\,0]$ is introduced on the $(\bar{1}\,\bar{1}\,1)$ plane, approximately 150 Angströms away from the CTB (Fig. 1b), using the free software Atomsk [32].

The perfect screw dislocation is introduced in the form of two half dislocations with $\boldsymbol{b} = \frac{a}{4}[1\,\bar{1}\,0]$ on the $(\bar{1}\,\bar{1}\,1)$ plane with an initial separation distance estimated from the isotropic elasticity of dislocations [21]. This ensures that the dissociation will lie in the $(\bar{1}\,\bar{1}\,1)$ plane and not in the (1 1 1) plane parallel to the CTB. The equilibrium configuration of the system obtained after energy minimization consists of two Shockley partials:

$$\frac{1}{2}\left[1\,\bar{1}\,0\right](BA) = \frac{1}{6}\left[1\,\bar{2}\,\bar{1}\right](B\gamma) + \frac{1}{6}\left[2\,\bar{1}\,1\right](\gamma A) \quad (1)$$

The separation distance between the partials is in reasonably

Table 1
Material parameters for the various EAM potentials for FCC metals.

Potential	μ [GPA]	b_p [Å]	γ_S [mJ.m^{-2}]	γ_{US} [mJ.m^{-2}]	γ_T [mJ.m^{-2}]	γ_{UT} [mJ.m^{-2}]
Al99	28	1.653	146	168	76	68
Al03	29.47	1.653	115	151	63	–
Al-LEA	29.4	1.646	128	163	58.1	54
Cu01	41.16	1.476	44	158	22.4	139
Cu12	43.55	1.486	45	233	22.2	245
Ni99	74.7	1.437	125	366	63	302

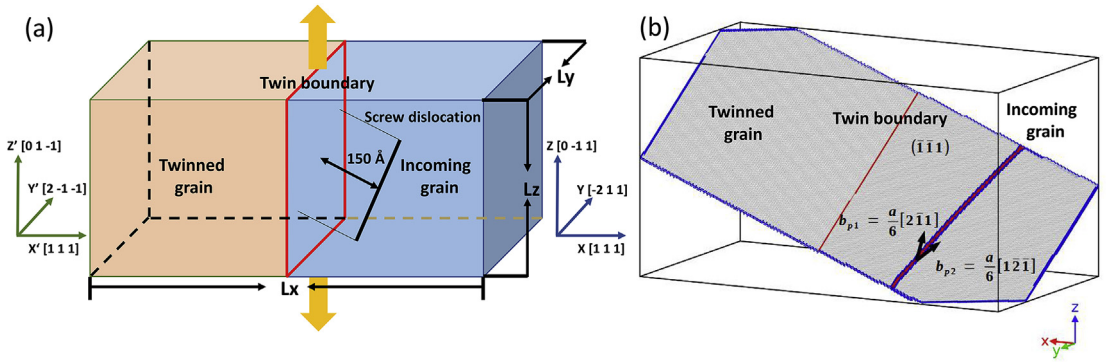

Fig. 1. (a) Schematic representation of the simulation cell. (b) Screw dislocation dissociated in two Shockley partials in the $(\bar{1}\,\bar{1}\,1)$ plane after relaxation. Atoms are colored based on the Common Neighbor Analysis where the FCC, HCP and other coordinated atoms appear in grey, red and blue respectively. Only the atoms in the $(\bar{1}\,\bar{1}\,1)$ plane are shown. (For interpretation of the references to color in this figure legend, the reader is referred to the Web version of this article.)

good qualitative agreement with the predicted equilibrium distance from anisotropic elasticity estimates [33–35] (Table C1). For the Al potentials it is also in reasonably good agreement with the 5.4 Å splitting distance predicted by Density Functional Theory (DFT) calculations [36].

2.3. Loading conditions

MD simulations were carried out with the open-source Large-scale Atomic/Molecular Massively Parallel Simulator (LAMMPS) [37] using a Nose-Hoover thermostat in the NVT ensemble. Simulations were performed at three different temperatures: 0.1K, 10K and 300K. As shown in Supplementary Material H, the trends presented in section 2 are not drastically affected by the temperature and most of the simulations presented in this manuscript are performed at 0.1K. Indeed, estimating the potential energy barriers associated to the interaction mechanisms (section 3) is more delicate at high temperature due to thermal fluctuations. Initially, a tensile loading is performed along the $[0\,\bar{1}\,1](CA)$ crystallographic direction, hereafter referred as z-tension. As illustrated in Fig. 1, the CTB plane is parallel to the loading direction, in other words there is no shear stress in the boundary plane. The loading is performed in stress-controlled mode by applying traction forces to the atoms in slabs with a width of 12 Å, which is larger than the cut-off radii of the potentials. Under such loading conditions, the screw dislocation experiences a high resolved shear stress (Schmid-Factor of 0.408) driving it towards the boundary, the driving force acting on the dislocation being given by the Peach-Koehler force [21]. The stress is applied in a single increment by applying opposite sign forces on the slabs at the positive and negative Z free surfaces. In order to minimize the stress fluctuations, the system is given an initial deformation which takes into account of both the elastic and thermal expansion. For a given applied stress, the components of the Voigt strain tensor are calculated from the Voigt stress tensor, and the atoms are displaced by a quantity $\Delta L_i = \varepsilon_{ij}.L_{ij}$, i and j taking the values for x, y or z and L being the length of the simulation cell in the i direction. Note that the Voigt tensor is different in the two grains.

For each stress state (*i.e.* loading condition), simulations are performed for several values of applied stress. On average, for a given loading condition, 6 simulation runs carried out at different magnitudes of applied stress are required to evaluate the critical transmission stress with a precision of $\pm$20 MPa. The repeatability of the MD simulations (interaction mechanism and of the critical stress for transmission) is assessed by repeating several times the same simulation run for a given applied stress. In total 150–200 simulation runs were carried-out for each potential.

In order to identify and interpret the interaction mechanisms, the potential energy of the atoms and the local atomic stress tensor are systematically computed using the virial formula [38]. The local crystalline structure is analyzed by the common neighbor analysis (CNA) [39], where FCC atoms, hexagonal close-packed (HCP) atoms and other coordinated atoms are colored in grey, red and blue respectively. The presence of an intrinsic stacking fault in between two partial dislocations is identified by two consecutives {1 1 1} planes of HCP atoms while a twin fault (*i.e.* the CTB) is identified by a single {1 1 1} HCP plane. The average energy per atom and local stress tensor of the dislocation/twin atoms discussed in section 3 are obtained by extracting the cohesive energy/local stress tensor of all the HCP and other coordinated atoms. The surface atoms are systematically discarded and the HCP atoms belonging to the CTB or to the stacking fault between the two partial dislocations are separated based on their spatial coordinates. Details on the calculation of these quantities can be found in supplementary material D. The open-source software 'Open Visualization Tool' (OVITO) [40] is used to visualize the atomic configurations. The dislocation analysis (DXA) [41] as implemented in Ovito is used to determine the Burgers vector of the dislocations. The line representation used in several figures of the manuscript is obtained with the same algorithms.

3. Results

3.1. Interaction mechanisms in Al, Cu and Ni under uniaxial tension

In this section, only the uniaxial tensile case is considered (z-tension). In Aluminum the dislocation reaction starts only after leading and trailing partials recombine into a perfect dislocation, *i.e.* the dislocation cross-slips onto the twin boundary plane via the Friedel-Escaig (FE) mechanism as illustrated in Fig. 2. Unlike in the quasi 2D simulations where the constriction occurs over the full length of the dislocation line [7,8], only a small fraction of the incoming dislocation constricts in the 3D geometry. As shown in Fig. 2a, this constriction occurs on the $(\bar{1}\,\bar{1}\,1)(\gamma)$ plane where a small screw segment (BA) is in contact with the CTB. After cross-slipping onto the CTB δ plane, the partials δA and $B\delta$, not being bound anymore by the SF, glide in opposite directions in the twin boundary plane (Fig. 2b), initiating the migration of the twin boundary by one atomic spacing. When the stress acting on the leading partial in the γ' plane (the dislocation glide plane in the twinned grain) reaches a critical value ($\sigma_{rss\_lead} > \sigma_{rss\_lead\_trans}$), the CTB Shockley partials cross-slip onto the γ' plane via the Fleischer mechanism (FL). The leading Shockley partial δA dissociates into a sessile stair rod-dislocation $\delta\gamma'$ and a glissile Shockley partial $\gamma' A$ that bows-out on the γ' plane, creating a stacking fault in the twinned grain (Fig. 2c). The cross-slip is completed by reaction of the trailing partial $B\delta$ with the stair rod dislocation, forming the trailing Shockley partial $B\gamma'$ gliding on the γ' plane (Fig. 2d).

Note that the bowing-out of the leading partial can also be observed below the critical transmission stress (Fig. 2e), however, the cross-slip nucleus rapidly dissolves (Fig. 2f), since both the elastic attractive forces and the SF surface tension act as driving forces for the resorption of the dislocation into the CTB.

The interaction forces between the screw dislocation and the CTB remain repulsive in Ni and Cu at short distances. Therefore, the driving force required to move the dislocation towards the CTB must counterbalance the repulsive force from the CTB as well as the image forces from the free surfaces [11]. The interaction mechanism starts here also only after the two Shockley partials γA and $B\gamma$ have constricted into a full dislocation BA. The transmission reveals a different scenario: as the incoming screw dislocation BA starts to interact with the CTB, cross-slip nuclei are observed simultaneously in the twin boundary plane (δA and $B\delta$ Shockley partials, absorption) and in the adjacent twinned grain ($\gamma' A$ and $B\gamma'$, transmission) as shown in Fig. 3a–b. The competition between slip transmission and absorption, both occurring by FE mechanism, suggests that both events must be energetically equivalent as was already suggested for Cu [11,12]. Whether transmission or absorption prevails depend on the magnitude of the resolved shear stress acting on the screw component of the BA dislocation on the γ' glide plane. Above the critical transmission stress ($\sigma_{rss\_screw} > \sigma_{rss\_screw\_trans}$ ~200 MPa) the cross-slip nucleus in the CTB dissolves in favor of the cross-slip nucleus in the twinned grain (Fig. 3c). Conversely, below the critical transmission stress the cross-slip nucleus in the twinned grain dissolves in favor of the cross-slip nucleus in the CTB (resorption into the CTB plane (Fig. 3d)).

In summary, 3D simulations under uniaxial tension reveal that curved dislocations can be transmitted in all three materials: in Al by a sequential mechanism involving both FE and FL mechanisms, in Ni/Cu by the FE mechanism alone.

This difference in the transmission mechanism implies that σ_{rss_trans} has to be defined as the resolved shear stress acting on the leading partial in Al since transmission occurs via the FL mechanism ($\sigma_{rss\_lead\_trans}$), whereas for Cu and Ni the resolved shear stress acting on the screw component (*i.e.* on the screw dislocation:

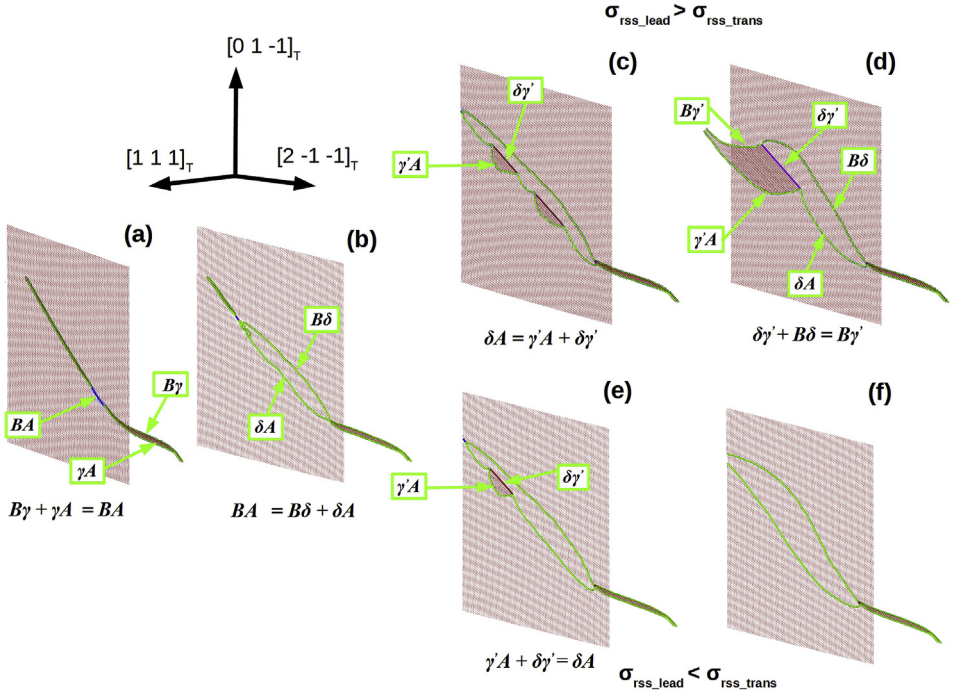

Fig. 2. *Interaction of incoming dislocation with the CTB in Al (Al99 potential, T = 10K).* (a) Constriction of the dislocation in contact with the CTB. (b) Cross slip into the CTB plane. (c) Transmission of the leading partial in the twinned grain for $\sigma_{rss\_lead} > \sigma_{rss\_trans}$. (d) Transmission of the trailing partial in the twinned grain for $\sigma_{rss\_lead} > \sigma_{rss\_trans}$. (e) Bowing out of a cross-slip nucleus for $\sigma_{rss\_lead} < \sigma_{rss\_trans}$. (f) Dissolution of the cross-slip nucleus for $\sigma_{rss\_lead} < \sigma_{rss\_trans}$. The atoms are colored according to the CNA analysis, only the non-FCC atoms are shown: the CTB is identified by a single HCP plane (red plane on the Figure). The dislocations are colored according to the DXA analysis, blue: perfect dislocation, green: Shockley partial and pink stair-rod dislocation. (For interpretation of the references to color in this figure legend, the reader is referred to the Web version of this article.)

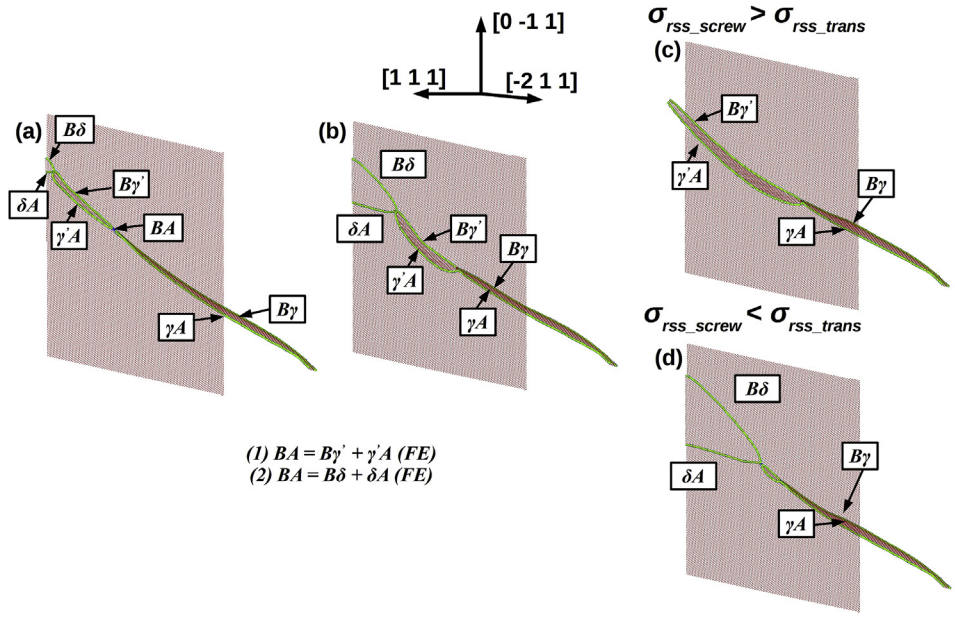

Fig. 3. *Interaction of the incoming dislocation with the CTB in Cu (Cu01 potential T = 0.1K).* (a,b) Competition between absorption on the δ CTB plane and transmission on the γ' plane (c) Transmission of the dislocation for $\sigma_{rss\_screw} > \sigma_{rss\_trans}$ (d) Absorption of the dislocation for $\sigma_{rss\_screw} < \sigma_{rss\_trans}$. The atoms are colored according to the CNA analysis, only the non-FCC atoms are shown. The dislocations are colored according to the DXA analysis, blue: perfect dislocation, green: Shockley partial dislocation. (For interpretation of the references to color in this figure legend, the reader is referred to the Web version of this article.)

$\sigma_{rss\_screw\_trans}$) is the relevant transmission stress since transmission occurs via FE.

Table 2 shows the values for the transmission stresses: the sequential transmission mechanism in Al occurs at a much larger stress (80% higher) than the FE transmission mechanism in Cu and Ni. Compared to the 2D simulations, the transmission in Cu and Ni occurs at significantly lower stresses which can be explained by geometrical considerations. In the quasi-2D case the two Shockley partials have to constrict over their full length into a perfect dislocation before they can interact with the CTB. In the 3D case, the curved dislocation forms a constriction node at its intersection with the CTB. This "point constriction" is achieved at a lower stress than the line constriction in quasi-2D. Furthermore, as shown in Fig. 4a, compressive regions can be observed in the CTB in the vicinity of the constriction nodes. These regions with high stress intensities can assist the transmission of the dislocation in the twinned grain. The fact that transmission is observed in the 3D Al simulations and not in the quasi 2D, can be explained with a similar argument: the partials in the CTB are bound by a stair rod representing compressive regions in the CTB. In other words, the 3D geometry allows more degrees of freedom in the spatial configuration of the dislocation line with respect to the CTB, facilitating transmission.

3.2. The influence of the loading conditions on the critical stress for transmission

In grain boundary networks, the stress experienced by the dislocations interacting with GBs is not uniaxial [26]. In this section we aim at understanding the influence of the stress state on the interaction mechanism/transmission stress. First, we focus on loading conditions producing no shear in the CTB such as z-tension, y-compression, pure yz-shear and yz-multiaxial loading with varying load ratios. Afterwards we look at the influence of shear in the CTB. Table 3 shows the Schmid factors for the $[1\,\bar{1}\,0](\bar{1}\,\bar{1}\,1)$, $[2\,\bar{1}\,1](\bar{1}\,\bar{1}\,1)$ and $[1\,\bar{2}\,\bar{1}](\bar{1}\,\bar{1}\,1)$ slip systems corresponding to the screw (BA/γ) dislocation, the leading ($\gamma A/\gamma$) and trailing partials ($B\gamma/\gamma$) respectively for the different loading conditions. By changing the stress state, the resulting stress acting on the leading and trailing partial dislocation is altered and so is the splitting distance or stacking fault between them. The effect can be represented by the Escaig stress (σ_{Escaig}), defined as the stress acting on the edge component of the Shockley partials, or in other words the resolved shear stress along the [1 1 2] ($D\gamma$) crystallographic direction.

Table 4 shows the Escaig stress for different loading conditions for the three materials. Given the geometry of the simulation, applying a compressive stress along the $[2\,\bar{1}\,\bar{1}](B\delta)$ crystallographic direction (y-compression) implies that a larger shear stress is acting on the trailing partial. The resulting negative Escaig stress tends to

Table 2
Critical stress for transmission for the three materials (z-tension) and comparison with the quasi-2D simulations.

σ_{rss_trans} (MPa)	*Al03*	*Cu01*	*Ni99*
3D, 0.1 K	480	260	255
Quasi-2D	No transmission	340 [12], 450 [8]	510 [8], 480 [7]

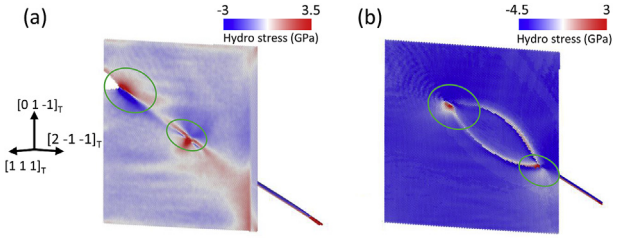

Fig. 4. *Atomic hydrostatic stress in the vicinity of the constriction node at 0.1K* (a) Cu01, $\sigma_{rss\_screw} = 200$ MPa (b) Al03, $\sigma_{rss\_lead} = 480$ MPa. The atoms are colored according to their local hydrostatic pressure as indicated by the associated color bar. Only the non-FCC atoms in the incoming grain are shown. (For interpretation of the references to color in this figure legend, the reader is referred to the Web version of this article.)

Table 3
Schmid factors for the screw, leading partial, trailing partial in the dislocation glide (incoming and twinned grain) and in the twin boundary plane for various loading conditions.

Loading conditions	Dislocation glide plane			Twin boundary plane		
	SF screw	SF lead	SF trail	SF screw	SF leading	SF trailing
z-tension	0.41	0.47	0.24	0	0	0
y-comp	0.41	0.31	0.39	0	0	0
yz-pure shear	0.47	0.27	0.55	0	0	0
xy-pure shear (matrix)	0.29	0.44	0.06	0.87	0.5	1
xy-pure shear (twin)	−0.29	−0.44	−0.06	−0.87	−0.5	−1

Table 4
Evolution of σ_{Escaig} under various loading conditions in Al, Cu and Ni. For each load ratio σ_{Escaig} is calculated at the critical stress for transmission.

Load ratio	Al		Ni		Cu	
	$\sigma_{rss\_lead\_trans}$(MPa)	σ_{Escaig} (MPa)	$\sigma_{rss\_screw\_trans}$(MPa)	σ_{Escaig} (MPa)	$\sigma_{rss\_screw\_trans}$(MPa)	σ_{Escaig} (MPa)
−10(σ_{yy})/-6(σ_{zz})	–	–	230	−320	–	–
−10/−3.4	–	–	–	–	299	−174
−10/−2	–	–	235	−93	285	−112
−10/0	–	–	240	−46	295	−56
−10/4.5	978	48	–	–	–	–
0/10	484	242	255	148	261	152
2/10	480	296	267	207	238	184
4.3/10	437	340	274	334	194	224
6.4/10	392	412	287	548	144	276

decrease of the separation distance between the partials. On the other hand, performing a uniaxial loading along the (*CA*) crystallographic direction (z-tension) (section 2.1) induces a larger stress on the leading partial or positive Escaig stress: the splitting distance between the partials increases. For a biaxial load ratio, the stress acting on the partials is controlled by the applied stress along the Y and Z directions, σ_{yy} and σ_{zz} respectively. For yz-biaxial compression, an increasing compressive stress along the Y direction decreases the Escaig stress (increase of the stress acting on the trailing partial and decrease of the stress acting on the leading partial). The opposite effect is observed for yz-biaxial tension where an increase of the tensile stress along the Y direction results in an increase of the Escaig stress (increase of the stress acting on the leading partial and decrease of the stress acting on trailing partial). For the three materials, Escaig stresses in the range −300 MPa/300 MPa for Ni and Cu and up to 430 MPa for Al are considered. Outside this range, the Schmid factor of the $[1\,\bar{1}\,0](\bar{1}\,\bar{1}\,1)$ (*BA*/*Υ*) slip system drops below 0.272, suggesting that under experimental conditions other easy slip systems would be activated and the dislocation would never operate.

Fig. 5 shows the critical transmission stress as a function of Escaig stress for the three materials. For Al a sharp decrease of the critical transmission stress is observed in the range 0 MPa $<\sigma_{Escaig}<$ 200 MPa, where $\sigma_{rss\_lead\_trans}$ drops from 980 MPa for σ_{Escaig} = 50 MPa (−10:4.5 load ratio) to 525 MPa for σ_{Escaig} = 200 MPa (−3:10 load ratio). For larger Escaig stresses between 200 MPa $<\sigma_{Escaig}<$ 430 MPa the critical transmission stress continues to decrease, though at a smaller rate: and reaches a value of 360 MPa for σ_{Escaig} = 430 MPa (7.2:10 load ratio). Transmission is not observed for negative Escaig stress *i.e.* when the dislocation is highly constricted in the incoming grain.

The situation is very different for Ni where the critical transmission stress is mostly independent of the Escaig stress: $\sigma_{rss\_screw\_trans}$ increases only from 230 MPa for σ_{Escaig} = −320 MPa (−10: 6 load ratio) to 275 MPa for σ_{Escaig} = 335 MPa (4.3:10 load ratio). Furthermore, transmission is still observed for negative Escaig stress.

Although the transmission mechanism in Cu is the same as in Ni

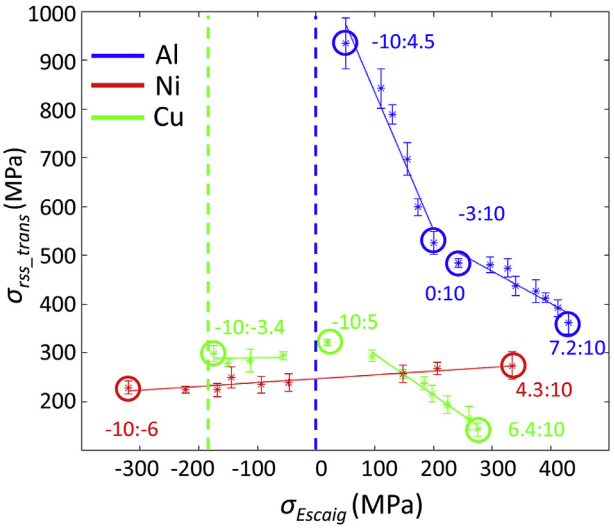

Fig. 5. Evolution of the critical transmission stress as a function of the Escaig stress in Al, Cu and Ni. The load ratios are specified for the circled points.

(FE mechanism), the critical transmission stress as function of the Escaig stress in Cu present more similarities with the Al case. For positive values of σ_{Escaig}, $\sigma_{rss\_screw\_trans}$ decreases with an increasing Escaig stress: from 320 MPa for σ_{Escaig} = 20 MPa (−10:5 load ratio) to 140 MPa for σ_{Escaig} = 280 MPa (6.4:10 load ratio), in other words the growth of cross-slip nuclei in the twinned grain is facilitated when the Escaig stress increases. For negative Escaig stresses in the range −180 MPa < σ_{Escaig} < 0 MPa transmission is nearly independent of Escaig and is observed at a critical stress of ~300 MPa. The growth of cross-slip nuclei is observed in the twin boundary plane and in the twinned grain with the latter dissolving in favor of the former when $\sigma_{rss\_screw} > \sigma_{rss\_screw\_trans}$. For $\sigma_{Escaig} < -180$ MPa, the growth of cross-slip nuclei in the twinned grain is no longer observed.

In summary, the dependence of the critical stress on the loading

conditions can be expressed as a function of the Escaig stress and is different for the three materials. In Ni the transmission stress is almost independent of the Escaig stress for the entire range of Escaig stresses considered. This is also the case in Cu for negative values of the Escaig stress. In Al and in Cu with increasing positive values of the Escaig stress transmission is facilitated in the twinned grain at a lower critical transmission stress. Furthermore, transmission is not observed for negative values of σ_{Escaig} in Al and for values below −180 MPa in Cu.

3.3. *The influence of a shear stress acting in the TB plane*

For a given load ratio (z-tension, y-compression, yz-biaxial tension …) we consider a resolved shear stress in the range [−400 MPa , 400 MPa] acting in the (1 1 1)(δ) TB plane. This is achieved by superimposing a xy-pure shear stress on top of the tensile/compressive/biaxial loading. The resulting Schmid Factors in the CTB plane (δ) for the $[1\,\bar{1}\,0](1\,1\,1)(BA/\delta)$ screw dislocation and the $[1\,\bar{2}\,1](1\,1\,1)(\delta A/\delta)$ leading and $[2\,\bar{1}\,\bar{1}](1\,1\,1)(B\delta/\delta)$ trailing partials are listed in Table 3 together with the Schmid factor in the γ and γ' plane for the perfect screw, leading and trailing partials.

Fig. 6 shows for the 4.3:10 load ratio (corresponding to σ_{Escaig} = 340 MPa without shear) the critical stress on the leading partial as a function of the Escaig stress and of the resolved shear stress on the CTB trailing partial ($\sigma_{rss\_trail\_CTB}$). As illustrated in Fig. 6a–b, $\sigma_{rss\_lead\_trans}$ remains constant in the range −200 MPa < $\sigma_{rss\_trail\_CTB}$ < 100 MPa. Outside this range, it gradually increases reaching a value of 500 MPa (12% increase) for $\sigma_{rss\_trail\_CTB} = \pm$ 300 MPa. This increase can be understood qualitatively using geometrical considerations. As illustrated in Fig. 6c a positive shear stress tends to push the trailing Shockley partial away from the stair-rod dislocation, hindering the dislocation reaction required for transmission of the trailing partial in the twinned grain. Note that the effect of shear has been calculated for several other load ratios (corresponding to different Escaig stresses) showing similar trends.

- The critical transmission stress remains constant over an interval centered around $\sigma_{rss\_trail\_CTB}$ = 0. The width of the plateau depends on the magnitude of Escaig stress at zero shear stress
- Large negative and positive shear stresses lead to an increase of the critical transmission stress

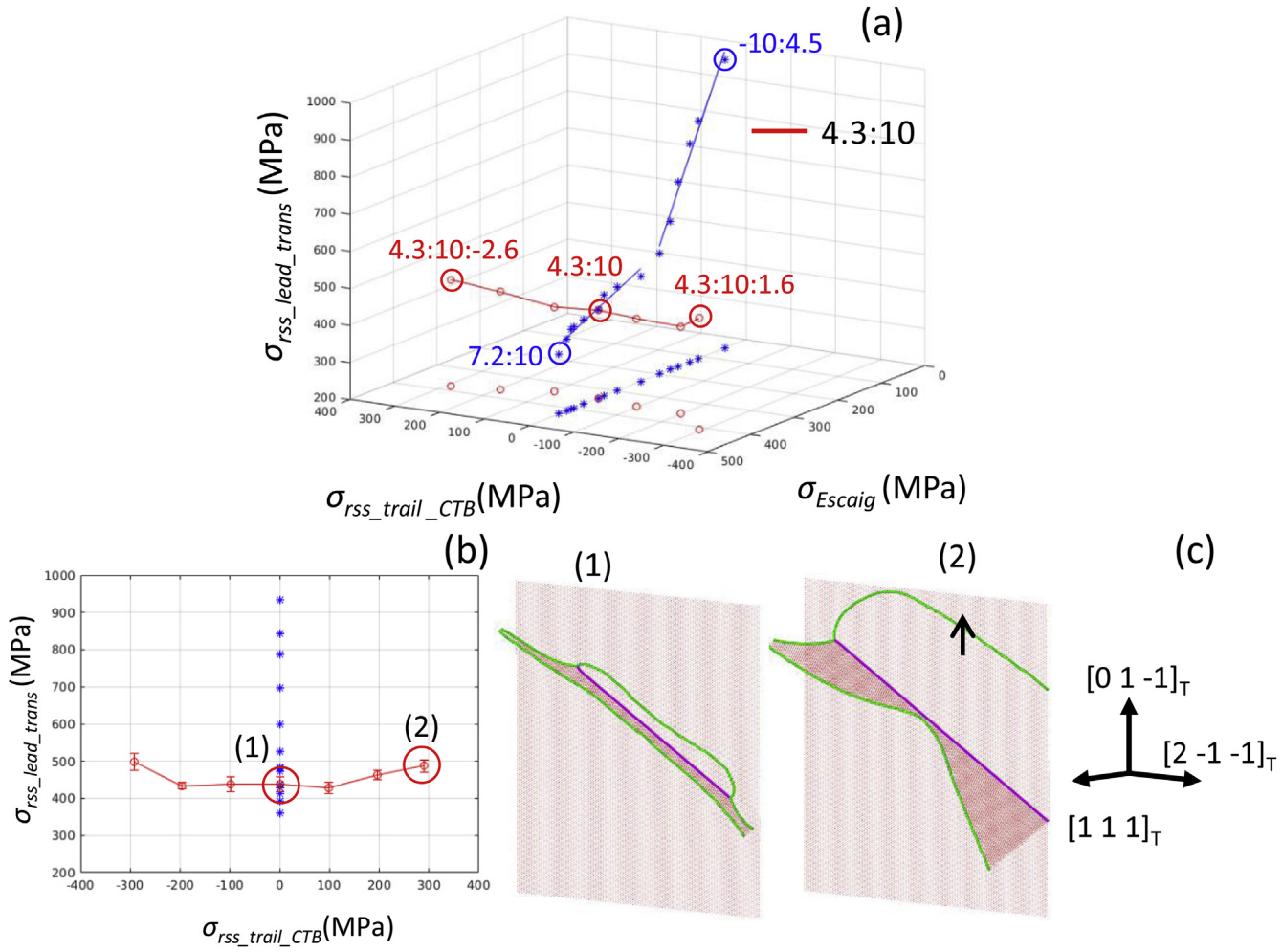

Fig. 6. *Influence of a shear stress in the CTB on the critical stress for transmission in Al.* (a) Critical transmission stress as a function of the Escaig stress and of the resolved shear stress acting on the trailing CTB partial. The blue data points are the same as in Fig. 5 (no shear stress in the CTB) while for the red data points a shear stress of varying magnitude is acting on the CTB. Load ratio(s) are indicated for the circled points and written as follows $\sigma_{yy}/\sigma_{zz}/\sigma_{xy}$ (b) Critical transmission stress as a function of the resolved shear stress acting on the trailing CTB partial (c) Effect of a resolved shear stress in the CTB plane on the transmission mechanism, snapshot are shown for the points circled in red in (b). The atoms/dislocations are colored according to the CNA/DXA analysis respectively only the non-FCC atoms are shown. (For interpretation of the references to color in this figure legend, the reader is referred to the Web version of this article.)

The influence of the shear stress in the TB plane is analogous in Cu and Ni as shown in Fig. 7 for the 0:10 load ratio (corresponding to $\sigma_{Escaig} = 150$ MPa in both cases). Despite the different transmission mechanism, the trends are very similar to those observed for Al. The stress remains fairly constant over an interval centered around $\sigma_{rss\_trail\_CTB} = 0$ MPa, slightly larger in width than in Al (−200 MPa/200 MPa, −200 MPa/300 MPa for Ni and Cu respectively). Outside this range an increase of σ_{rss_trans} is observed. While a smooth parabolic curve is obtained for Ni, a larger scatter observed for Cu. The latter is related to boundary effects: *e.g.* the sharp increase around $\sigma_{rss\_trail\_CTB} = 320$ MPa is related to the absorption of a part of the trailing CTB partial at the free surfaces. Once this absorption occurs, the recombination energy of the CTB partials drastically increases, making the growth of the twin boundary cross-slip nucleus more favorable energetically. For both materials, the increase of the critical transmission stress under the effect of a shear stress in the TB plane can be attributed to the work done on the partial dislocations, decreasing of the energy of the cross-slip nucleus in the TB plane and favoring the growth of the cross-slip nucleus in the twin boundary plane at the expense of the cross-slip nucleus in the twinned grain.

4. Discussion

The nature of the interaction force between the CTB and the dislocation in the three materials plays an important role in the transmission behavior. To estimate the potential energy barrier associated with this interaction, we calculate the average cohesive energy per atom of the dislocation $< E_{dislo} >_{atoms}$, including the stacking fault ribbon and the parameter $< E_{core} >_{atoms}$, including solely the dislocation core atoms. The latter being defined as the non-12-coordinated atoms in the vicinity of the dislocation core (as determined by the CNA analysis).

The calculation of $< E_{core} >_{atoms}$ is rather straightforward; independently of the state of the dislocation (propagating into the original or twinned grains, or absorbed into the CTB), all the core atoms are taken into account while the HCP atoms are systematically discarded:

$$< E_{core} >_{atoms} = \frac{\left(\sum_i^{Ncore} E_i\right)}{N_{core}} \quad (2)$$

Where N_{core} is the total number of atoms belonging to the

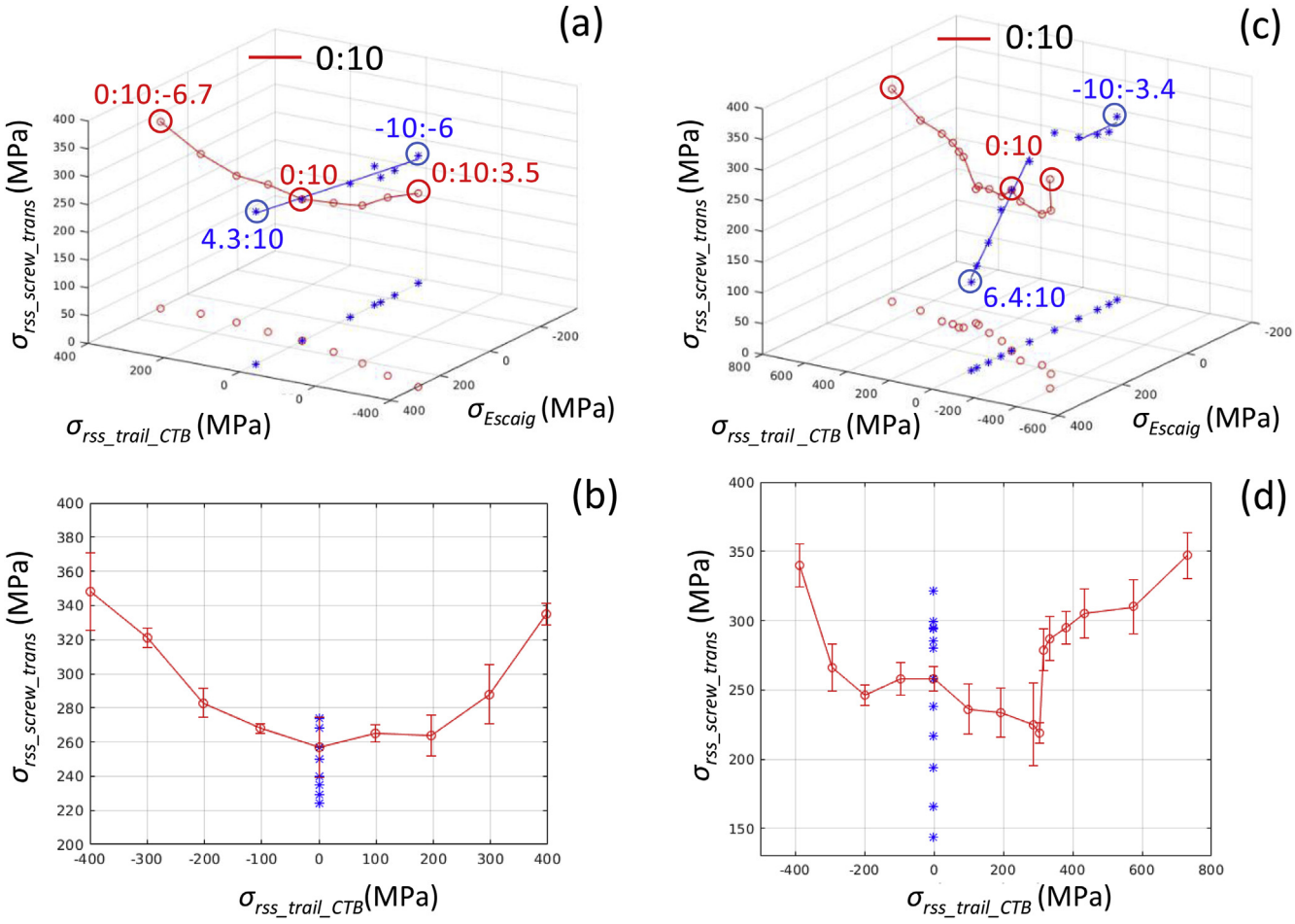

Fig. 7. *Influence of a shear stress in the CTB on the critical stress for transmission in Cu and Ni.* Critical transmission stress as a function of the Escaig stress and of the resolved shear stress acting on the trailing CTB partial in Ni (a) and Cu (c) The blue data points are the same as in Fig. 5 (no shear stress in the CTB) while for the red data points a shear stress of varying magnitude is acting on the CTB. Load ratio(s) are indicated for the circled points and written as follows $\sigma_{yy}/\sigma_{zz}/\sigma_{xy}$. Critical transmission stress as a function of the resolved shear stress acting on the trailing CTB partial in Ni (b) and Cu (d). (For interpretation of the references to color in this figure legend, the reader is referred to the Web version of this article.)

dislocation core and E_i is the cohesive energy of atom i.

Similarly to $<E_{core}>_{atoms}$, $<E_{dislo}>_{atoms}$ includes all the core atoms, as well as the HCP atoms belonging to the stacking fault ribbon between the two Shockley partials (Fig. D1a). On the other hand, when the dislocation is absorbed into the CTB, the partial dislocations are no longer bound by the SFE and can propagate along opposite directions on the twin boundary plane. Doing so, the HCP atoms between the twinning partials are displaced by one atomic spacing (Fig. D1b). These HCP atoms are no longer part of the dislocation and are systematically discarded. Therefore, $<E_{dislo}>_{atoms}$ is calculated as follows:

$$<E_{dislo}>_{atoms} = \frac{\left(\sum_j^{Ncore \notin CTB} E_j + \sum_k^{Ncore \in CTB} E_k + \sum_l^{Nhcp \notin CTB} E_l\right)}{N_{core \notin CTB} + N_{core \in CTB} + N_{hcp \notin CTB}} = \frac{\left(\sum_i^{Ncore} E_i + \sum_l^{Nhcp \notin CTB} E_l\right)}{N_{core} + N_{hcp \notin CTB}} \quad (3)$$

Where $N_{hcp \notin CTB}$ is the total number of atoms belonging to the stacking fault ribbon.

Note that simplified expression for $<E_{dislo}>_{atoms}$ can be derived when all the dislocation atoms are either all in the original/twinned grain (eq. (D3)) or absorbed into the CTB (eq. (D4)).

Further details in the methodology for the calculation of this quantity are given in Supplementary material D.

4.1. Uniaxial deformation

Fig. 8a–b shows for all potentials used $<E_{dislo}>_{atoms}$ and $<E_{core}>_{atoms}$ as a function of time for a resolved shear stress below the transmission threshold ($\sigma_{rss} < \sigma_{rss\_trans}$). To allow a quantitative comparison the same applied stress is used for the three Al potentials. The difference between the energy of the dislocation in the incoming grain and in the CTB is called ΔE_{abs}. Calculation details of this quantity as well as its values for the six potentials are provided in Supplementary material D and Table E1 respectively. Two opposite trends are observed: $\Delta E_{abs} < 0$ for all three Al potentials while $\Delta E_{abs} > 0$ for the two Cu and the Ni potential. Although less pronounced, similar trends are observed for $<E_{core}>_{atoms}$: absorption into the CTB results in a large decrease of the core energy in Al and a slight increase in Cu and Ni. These differences are related to the nature of the interaction force between the incoming screw dislocation and the CTB. In Al, this force is attractive at short distances: the core energy of the dislocation decreases upon absorption. In Ni and Cu, the force remains repulsive at short distances: absorption of the screw dislocation results in a slight increase of the dislocation core energy (Fig. 8b). The stacking fault energy also influences $<E_{dislo}>_{atoms}$ and the corresponding ΔE_{abs}. Since the CTB Shockley partials are not bound by a stacking fault in the CTB, the energy difference between the dislocation in CTB and the dislocation in the grain will be higher in materials with high stacking fault energy such as Al. Overall, the computation of $<E_{dislo}>_{atoms}$ evidences that cross-slip of the dislocation in the CTB in Al is energetically more favorable, the CTB act as a sink for screw dislocations, and therefore a large driving force (*i.e.* a large resolved shear stress) is required to promote transmission into the twinned grain. On the other hand, in Cu and Ni, the increase of $<E_{dislo}>_{atoms}$ upon absorption suggests that this mechanism is not energetically as favorable, explaining the competition between transmission and absorption as observed in Fig. 5.

4.2. Influence of the loading conditions on the energy barrier for transmission

Also for the multiaxial case without shear in the CTB, the evolution of $<E_{dislo}>_{atoms}$ for different loading conditions, representing different Escaig stresses, allows gaining further understanding in the observed trends in the critical transmission stress. Fig. 9a–b shows the evolution of $<E_{dislo}>_{atoms}$ as a function of time for Al and Ni for different loading conditions this time for an applied stress above the transmission threshold: $\sigma_{rss} > \sigma_{rss\_trans}$. When the dislocation transmits in the twinned region, one can calculate the

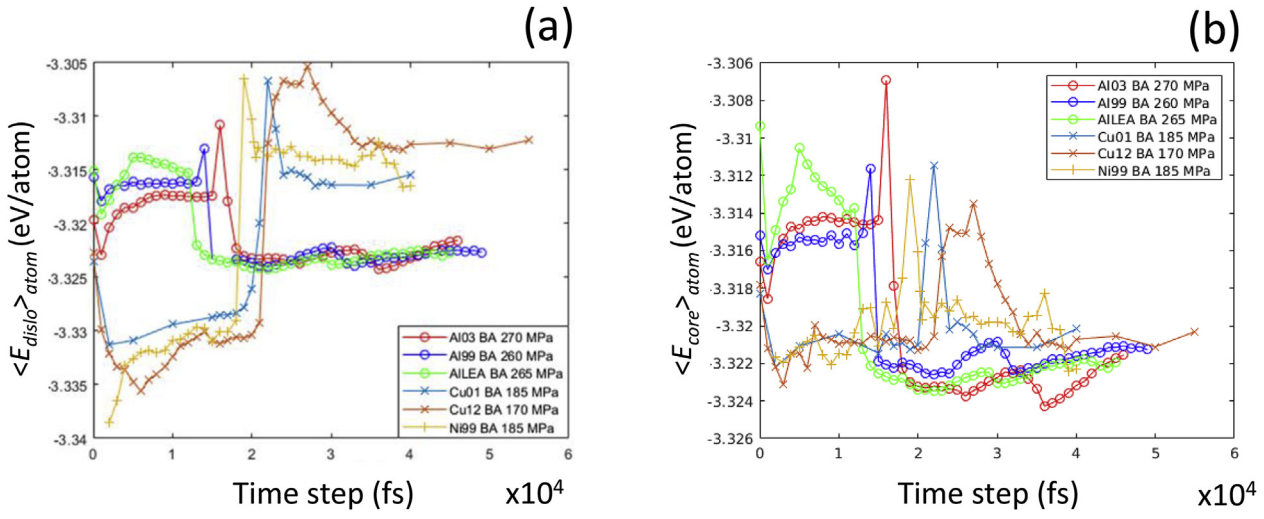

Fig. 8. (a) Evolution of $<E_{dislo}>_{atoms}$ for the six potentials below the transmission threshold for the six potentials (b) Evolution of the core energy below the transmission threshold. The plots are centered on the same average value to allow an easier comparison of ΔE_{abs}.

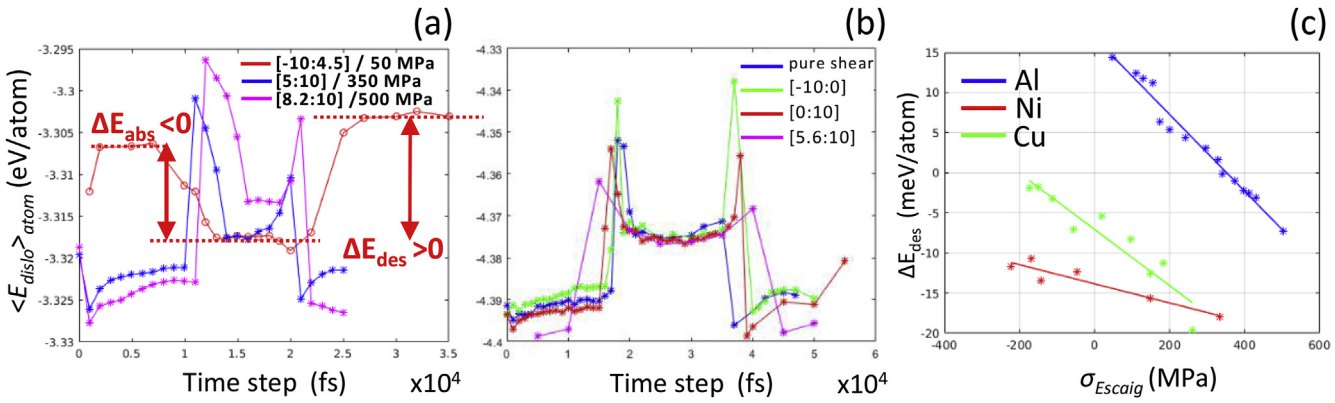

Fig. 9. Evolution of $<E_{dislo}>_{atoms}$ as a function of time in (a) Al for $\sigma_{rss\_lead} > \sigma_{rss\_trans}$ (σ_{Escaig} is indicated for each stress state) (b) Ni for $\sigma_{rss\_screw} > \sigma_{rss\_trans}$ (c) Evolution of ΔE_{des} as a function of the Escaig stress in Al, Ni, Cu.

difference between the energy of the dislocation in the CTB and in the twinned grain, hereafter referred as ΔE_{des}. This quantity is representative of the energy barrier for desorption and in the absence of shear in the CTB, the stresses acting on the partials are the same in the incoming grain and in the twinned grain and $\Delta E_{des} \sim -\Delta E_{abs}$.

In Al, since the incoming screw dislocation systematically cross-slips in the CTB by FE before being transmitted in the twinned grain by FL, the energy barrier for desorption ΔE_{des} is also the energy barrier for transmission. In Cu and Ni however, cross-slip nuclei are observed in the CTB and the twinned grain simultaneously *i.e.* cross-slip onto the CTB is not required for transmission. For these two materials, ΔE_{des} rather assesses the relative stability of the cross-slip nuclei in the CTB and twinned grain. Nevertheless, we will consider in a first approach ΔE_{des} for all three materials as function of the Escaig stress and relate this behavior to the critical transmission stress (Fig. 9c). Smaller effects related to the spatial configuration of the dislocations in the CTB will be discussed additionally. In the incoming and outgoing grains, $<E_{dislo}>_{atoms}$ depends on the splitting distance between the Shockley partials (Fig. F1). When the stress acting on the trailing partial is larger than the stress on the leading ($\sigma_{Escaig} < 0$), the small splitting distance results in a large value of $<E_{dislo}>_{atoms}$.

In such a case, the energy barrier for absorption is low while the energy barrier for desorption is high. Conversely, when the stress acting on the leading partial is larger than the stress acting on the trailing partial ($\sigma_{Escaig} > 0$), the large splitting distance results in a low value of $<E_{dislo}>_{atoms}$: in such a case the energy barrier for absorption is high while the energy barrier for desorption is low. According to these considerations and independently of the material considered, the critical stress for transmission is expected to decrease for an increasing Escaig stress. Why does the dependence of the critical stress for transmission on the Escaig stress differ so much from one material to another?

The splitting distance is strongly dependent on the Escaig stress in Al (Fig. F1b): and therefore changing the loading conditions induces large variations of $\Delta E_{abs,des}$. Fig. 9a shows that ΔE_{des} varies between 14.4 meV/atom for $\sigma_{Escaig} = 50$ MPa (−10:4.5 load ratio) and only −6.9 meV/atom for $\sigma_{Escaig} = 480$ MPa (8.2:10 load ratio). In Ni, on the other hand, the splitting distance is weakly dependent on the Escaig stress: changing the loading conditions barely affects $\Delta E_{abs,des}$. This is illustrated in Fig. 9b where ΔE_{des} varies between −13.5 meV/atom for $\sigma_{Escaig} = -145$ MPa (pure shear yz) and −18 meV/atom for $\sigma_{Escaig} = 335$ MPa (5.6:10 load ratio).

These trends are summarized in Fig. 9c which shows that ΔE_{des} decreases linearly with the Escaig stress for the three materials, however the slopes are different: Al and Cu exhibit a strong dependence on Escaig while a weak dependence is observed for Ni.

The influence of the Escaig stress is schematically illustrated for Al in Fig. 10. As discussed in section 2, absorption in Al is extremely favorable energetically and occurs spontaneously. However, for very high Escaig stresses, absorption could become unfavorable energetically ($\Delta E_{abs} >> 0$). In such a case it is expected that the transmission mechanism would become similar to the one observed in Ni and Cu, *i.e.* occurring via the FE mechanism and not requiring the initial absorption of the dislocation into the CTB. This scenario has not been observed in the range of Escaig stresses considered in this work; however in the range considered in this study, ΔE_{des} has a strong influence on the critical stress for transmission. Indeed, the driving force *i.e.* the stress on the leading Shockley partial required to overcome the energy barrier and promote the growth of the cross-slip nucleus in the twinned grain decreases with increasing Escaig stress (as shown in Fig. 5). For a given biaxial load ratio, the ratio between the stress acting on the leading and the trailing partial remains constant when varying the applied stresses along the Y and Z direction. As a consequence, if the stress acting on the leading partial is larger than the stress acting on the trailing ($\sigma_{Escaig} > 0$ MPa), increasing the applied stress results in a decrease of $<E_{dislo}>_{atoms}$ and the desorption barrier can be overcome providing that the driving force is sufficiently large ($\sigma_{rss\_lead} > \sigma_{rss\_trans}$). The situation is different when the stress acting on the trailing is larger than the stress acting on the leading ($\sigma_{Escaig} < 0$). For such values of σ_{Escaig} the dislocation is highly constricted, *i.e.* ΔE_{des} has a large value. Overcoming this desorption barrier would imply to provide a large driving force, *i.e.* to increase the stress acting on the leading partial. However, for $\sigma_{Escaig} < 0$ increasing the stress acting on the leading partial also implies further decreasing the Escaig stress. In other words, for a given load ratio, increasing the applied stress also increases the strength of the desorption barrier: the dislocation cannot escape from the CTB for $\sigma_{Escaig} < 0$ MPa (corresponding to $\Delta E_{des} > 17$ meV in Al). Note that the stress acting on the partials controls the spatial configuration of the dislocation upon interaction with the CTB. As a consequence, the number of constriction nodes or the length of the stair-rod segment when $\sigma_{rss\_lead} > \sigma_{rss\_trans}$ depend on the stress acting on the Shockley partials in the incoming grain. These effects will also alter the value of ΔE_{abs} for a given Escaig stress (supplementary material G).

In Ni on the other hand, the absorption barrier remains high, even when the Escaig stress reaches large negative values (−10: 6 load ratio, $\sigma_{Escaig} = -320$ MPa, $\Delta E_{abs} = 9.8$ meV/atom). Around the critical transmission stress, a large fraction of the incoming

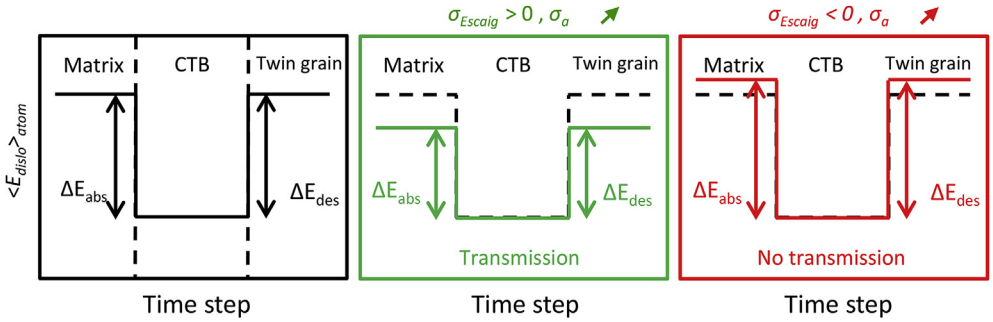

Fig. 10. Evolution of the magnitude of ΔE_{des} upon increasing the applied stress for $\sigma_{Escaig} > 0$ MPa and $\sigma_{Escaig} < 0$ MPa.

dislocation segment is systematically transmitted in the twinned grain. This is illustrated in Fig. 11a where the growth of a large cross-slip nucleus is still observed for extremely large negative values of the Escaig stress ($\sigma_{Escaig} = -907$ MPa). Independently of the Escaig stress, the nucleation of the cross-slip nuclei in the CTB is always initiated in the vicinity of the free surfaces. For $\sigma_{rss\_lead} < \sigma_{rss\_trans}$ the cross-slip nucleus in the twinned grain gradually dissolves in favor of the cross-slip nuclei in the CTB (resorption), however, the initial growth of the cross-slip nucleus is observed independently of the Escaig stress (Fig. 11a–b). Interestingly, the slopes of $\sigma_{rss\_trans} = f(\sigma_{Escaig})$ and $\Delta E_{des} = f(\sigma_{Escaig})$ have an opposite sign in the case of Ni, *i.e.*, while the slight decrease of ΔE_{des} with an increasing Escaig stress should result in a slight decrease of σ_{rss_trans}, the opposite trend is observed. This tends to indicate that the critical transmission stress is also influenced by parameters that are not captured by the calculation of ΔE_{des} (such as the work done on the Shockley partials for instance).

Due to the sensitivity of $\Delta E_{abs}/\Delta E_{des}$ to the Escaig stress in Cu, the transmission behavior in Cu exhibits similarities with Al. The decrease of σ_{rss_trans} observed for an increasing $\sigma_{Escaig} > 0$ MPa, is also correlated to the increase/decrease of $\Delta E_{abs}/\Delta E_{des}$ respectively. The increase of ΔE_{abs} favors the initial growth of the cross-slip nucleus in the twinned grain and the decrease of ΔE_{des} favors the desorption of the CTB Shockley partials in the twinned grain. These two mechanisms explain the decrease of σ_{rss_trans} with increasing σ_{Escaig}.

Additionally, due to the rapid decrease of ΔE_{abs} with decreasing Escaig stress, there is also a critical stress below which transmission can no longer be observed. Interestingly, for $\sigma_{Escaig} < 0$ MPa, there is no obvious correlation between ΔE_{des} and σ_{rss_trans}: while ΔE_{des} increases with decreasing Escaig stress, σ_{rss_trans} remains constant around 300 MPa.

The interaction mechanism depends on the Escaig stress:

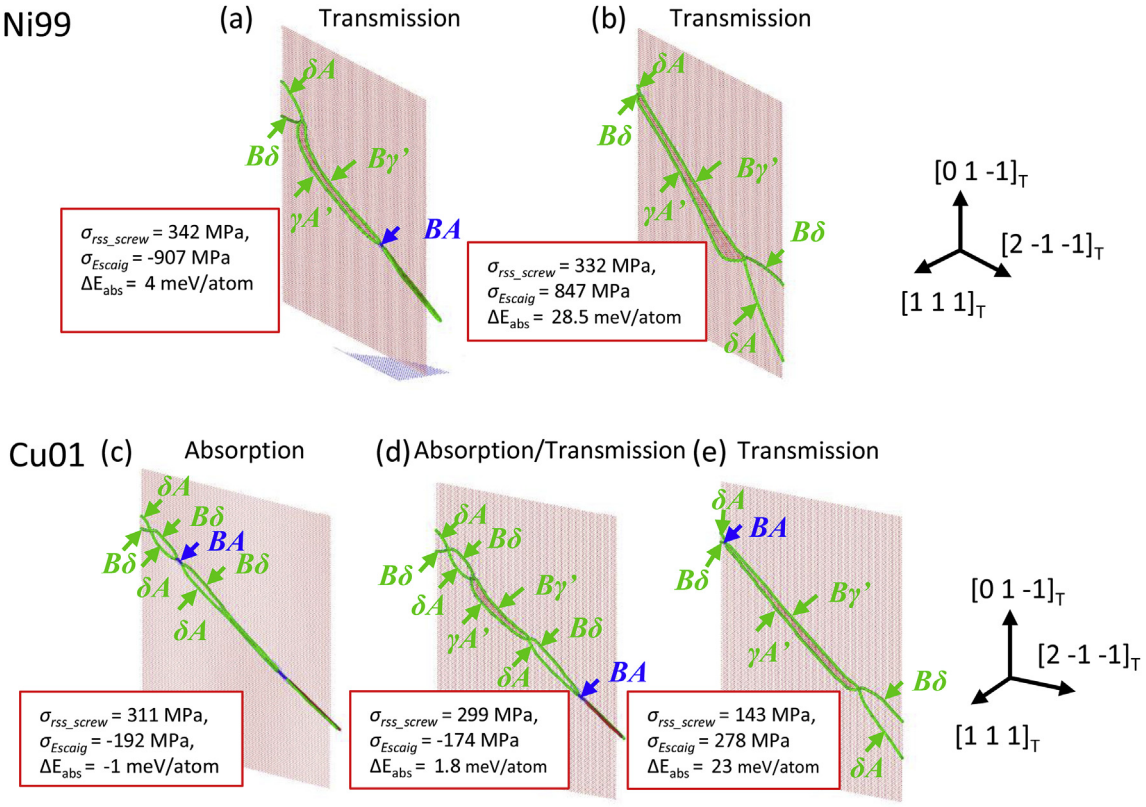

Fig. 11. Nucleation and growth of the cross-slip nuclei in the TB and in the TG as a function of the Escaig stress for Ni and Cu.

- For large positive values of σ_{Escaig} ($\sigma_{Escaig} > 100$ MPa), corresponding to large values of ΔE_{abs} ($\Delta E_{abs} > 10$ meV/atom), the growth of a large cross-slip nucleus is systematically observed in the twinned grain. The nucleation of cross-slip nuclei in the CTB is only observed in the vicinity of the free surfaces (Fig. 11e). In this range of Escaig stresses, the interaction mechanism is similar to the one observed in Ni.
- For -180 MPa $< \sigma_{Escaig} < 100$ MPa, ΔE_{abs} quickly decreases with the decreasing Escaig stress and absorption becomes increasingly favorable energetically. The nucleation of cross-slip nuclei in the CTB is now also observed far away from the free surfaces. In this range of σ_{Escaig}, nucleation and growth of cross-slip nuclei in the twinned grain and in the twin boundary are energetically equivalent, there is a competition between slip transmission and absorption (Fig. 11d) and transmission prevails over absorption for $\sigma_{rss\_screw} > \sigma_{rss\_trans}$.
- For $\sigma_{Escaig} < -180$ MPa, absorption is energetically favorable ($\Delta E_{abs} < 0$) while desorption becomes unfavorable ($\Delta E_{des} > 0$). In this range of Escaig stresses, the energy of a cross-slip nucleus in the twin boundary is significantly lower than the energy of a cross-slip nucleus in the twinned grain: even if a large stress acts on the screw dislocation, transmission is no longer observed (Fig. 11c).

The interaction mechanism is here similar to the case of Al for $\sigma_{Escaig} < 0$. When the stress acting on the trailing Shockley is larger than the stress acting on the leading, *i.e.* $\sigma_{Escaig} < 0$, increasing the stress on the screw component also implies decreasing the Escaig stress, or in other words increasing the magnitude of the desorption barrier. As a consequence, if the critical stress (~300 MPa for $\sigma_{Escaig} < 0$ in Cu) is reached for $\sigma_{Escaig} < -180$ MPa, the CTB Shockley partials are not able to overcome the large desorption barrier and can't escape from the CTB: transmission is not observed.

The evolution of the transmission behavior for the −10: 2 load ratio provides a good illustration of these trends.

- For $\sigma_{rss\_screw} < 300$ MPa, nucleation of cross-slip nuclei is observed in the CTB and in the twinned grain, but the latter eventually dissolve in favor of the former: the driving force (*i.e.* the stress acting on the screw component) is not large enough to promote transmission in the twinned grain
- For 300 MPa $< \sigma_{rss\_screw} < 450$ MPa corresponding to -180 MPa $< \sigma_{Escaig} <$ -115 MPa, the incoming dislocation is transmitted in the twinned region since $\sigma_{rss\_trans} > \sigma_{rss\_screw}$
- For $\sigma_{rss\_screw} > 450$ MPa corresponding to $\sigma_{Escaig} <$ -180 MPa, transmission is no longer observed: both the energy of the cross-slip nucleus in the twinned grain and the desorption barrier are very high, despite the large stress acting on the screw component, absorption is always more favorable energetically.

Overall, transmission becomes increasingly difficult when increasing the compressive stress acting along the Y direction. Transmission is for instance never observed for the −10: 4.2 load ratio: indeed, for this load ratio σ_{Escaig} = -225 MPa, *i.e.* much lower than the limit of −180 MPa for which the critical stress on the screw component is reached.

5. Conclusion

Large 3D simulations with free boundary conditions performed to investigate the interaction mechanism between a screw dislocation and a coherent twin boundary revealed the influence of the dislocation curvature and the length of the dislocation segment that cannot be captured in quasi 2D simulations. The interaction mechanism and transmission stress depend on the material considered:

- In Al, absorption is energetically favorable; nevertheless, direct transmission at large applied stress can occur via a sequential transmission process using both FL and FE mechanism.
- In Ni and Cu, there is a competition between transmission and absorption above the critical stress for interaction, both mechanisms occurring via the FE mechanism. Complete transmission in the twinned grain is observed at an applied stress almost twice as low as the values reported in the quasi-2D simulations (200 MPa vs 400 MPa).

The influence of the multiaxial loading conditions on the critical transmission stress was investigated and the results are interpreted in terms of the Escaig stress. Both Al and Cu show a large dependence to the Escaig stress, while in Ni, the critical transmission stress is almost constant over a large range of Escaig stresses. In all materials, the presence of a shear stress in the CTB tends to increase the critical transmission stress. The observed trends were correlated with the potential energy barrier associated with this interaction, which is obtained by the calculation of the average cohesive energy per atom in the dislocation. Overall the evolution of the critical transmission stress is well correlated to the evolution of these potential energy barriers for the three materials.

Acknowledgments

HVS and MD gratefully thank the European Research Council for the financial support within the advanced grant advanced grant MULTIAX (339245). The authors would also like to thank the Swiss Supercomputing Centre for access to the Piz Daint cluster where the MD simulations were performed. Work by SIR was supported through the Air Force onsite contract No. FA8650-15-D-5230 managed by UES, Inc., USA.

Appendix A. Supplementary data

Supplementary data to this article can be found online at https://doi.org/10.1016/j.actamat.2019.05.025.

References

[1] T.H. Blewitt, R.R. Coltman, J.K. Redman, Low-temperature deformation of copper single crystals, J. Appl. Phys. 28 (1957) 651–660, https://doi.org/10.1063/1.1722824.
[2] L. Lu, Y. Shen, X. Chen, L. Qian, K. Lu, Ultrahigh strength and high electrical conductivity in copper, Science 304 (2004) 422–426, https://doi.org/10.1126/science.1092905.
[3] Y.F. Shen, L. Lu, Q.H. Lu, Z.H. Jin, K. Lu, Tensile properties of copper with nanoscale twins, Scripta Mater. 52 (2005) 989–994, https://doi.org/10.1016/j.scriptamat.2005.01.033.
[4] P.J. Imrich, C. Kirchlechner, C. Motz, G. Dehm, Differences in deformation behavior of bicrystalline Cu micropillars containing a twin boundary or a large-angle grain boundary, Acta Mater. 73 (2014) 240–250, https://doi.org/10.1016/j.actamat.2014.04.022.
[5] J.P. Couzinié, B. Décamps, L. Priester, Interaction of dissociated lattice dislocations with a Σ=3 grain boundary in copper, Int. J. Plast. 21 (2005) 759–775, https://doi.org/10.1016/j.ijplas.2004.04.013.
[6] J.P. Couzinié, B. Decamps, L. Priester, On the interactions between dislocations and a near-Σ=3 grain boundary in a low stacking-fault energy metal, Phil. Mag. Lett. 83 (2003) 721–731, https://doi.org/10.1080/09500830310001614522.
[7] M. Chassagne, M. Legros, D. Rodney, Atomic-scale simulation of screw dislocation/coherent twin boundary interaction in Al, Au, Cu and Ni, Acta Mater. 59 (2011) 1456–1463, https://doi.org/10.1016/j.actamat.2010.11.007.
[8] Z.-H. Jin, P. Gumbsch, E. Ma, K. Albe, K. Lu, H. Hahn, H. Gleiter, The interaction mechanism of screw dislocations with coherent twin boundaries in different face-centred cubic metals, Scripta Mater. 54 (2006) 1163–1168, https://doi.org/10.1016/j.scriptamat.2005.11.072.
[9] Z.-H. Jin, P. Gumbsch, K. Albe, E. Ma, K. Lu, H. Gleiter, H. Hahn, Interactions between non-screw lattice dislocations and coherent twin boundaries in face-centered cubic metals, Acta Mater. 56 (2008) 1126–1135, https://doi.org/

10.1016/j.actamat.2007.11.020.
[10] X. Zhang, A. Misra, H. Wang, M. Nastasi, J.D. Embury, T.E. Mitchell, R.G. Hoagland, J.P. Hirth, Nanoscale-twinning-induced strengthening in austenitic stainless steel thin films, Appl. Phys. Lett. 84 (2004) 1096–1098, https://doi.org/10.1063/1.1647690.
[11] Z. Chen, Z. Jin, H. Gao, Repulsive force between screw dislocation and coherent twin boundary in aluminum and copper, Phys. Rev. B 75 (2007) 212104, https://doi.org/10.1103/PhysRevB.75.212104.
[12] T. Zhu, J. Li, A. Samanta, H.G. Kim, S. Suresh, Interfacial plasticity governs strain rate sensitivity and ductility in nanostructured metals, Proc. Natl. Acad. Sci. Unit. States Am. 104 (2007) 3031–3036, https://doi.org/10.1073/pnas.0611097104.
[13] M.J. Buehler, A. Hartmaier, H. Gao, Hierarchical multi-scale modelling of plasticity of submicron thin metal films, Model. Simul. Mater. Sci. Eng. 12 (2004) S391, https://doi.org/10.1088/0965-0393/12/4/S07.
[14] Y. Zheng, J. Lu, H. Zhang, Z. Chen, Strengthening and toughening by interface-mediated slip transfer reaction in nanotwinned copper, Scripta Mater. 60 (2009) 508–511, https://doi.org/10.1016/j.scriptamat.2008.11.039.
[15] L. Li, N.M. Ghoniem, Twin-size effects on the deformation of nanotwinned copper, Phys. Rev. B 79 (2009), 075444, https://doi.org/10.1103/PhysRevB.79.075444.
[16] I. Shabib, R.E. Miller, Deformation characteristics and stress–strain response of nanotwinned copper via molecular dynamics simulation, Acta Mater. 57 (2009) 4364–4373, https://doi.org/10.1016/j.actamat.2009.05.028.
[17] Z.X. Wu, Y.W. Zhang, D.J. Srolovitz, Dislocation–twin interaction mechanisms for ultrahigh strength and ductility in nanotwinned metals, Acta Mater. 57 (2009) 4508–4518, https://doi.org/10.1016/j.actamat.2009.06.015.
[18] X. Li, Y. Wei, L. Lu, K. Lu, H. Gao, Dislocation nucleation governed softening and maximum strength in nano-twinned metals, Nature 464 (2010) 877–880, https://doi.org/10.1038/nature08929.
[19] S. Xu, L. Xiong, Y. Chen, D.L. McDowell, Sequential slip transfer of mixed-character dislocations across Σ3 coherent twin boundary in FCC metals: a concurrent atomistic-continuum study, Npj Computational Materials 2 (2016) 15016, https://doi.org/10.1038/npjcompumats.2015.16.
[20] T. Ezaz, M.D. Sangid, H. Sehitoglu, Energy barriers associated with slip–twin interactions, Phil. Mag. 91 (2011) 1464–1488, https://doi.org/10.1080/14786435.2010.541166.
[21] J. Hirth, J. Lothe, Theory of Dislocations, John Wiley \& Sons, 1982.
[22] R.L. Fleischer, Cross slip of extended dislocations, Acta Metall. 7 (1959) 134–135, https://doi.org/10.1016/0001-6160(59)90122-1.
[23] M.S. Duesbery, Dislocation motion, constriction and cross-slip in fcc metals, Model. Simul. Mater. Sci. Eng. 6 (1998) 35, https://doi.org/10.1088/0965-0393/6/1/005.
[24] J. Friedel, Dislocations and Mechanical Properties of Crystals, J. Wiley Sons, New York, NY, 1957.
[25] B. Escaig, Sur le glissement dévié des dislocations dans la structure cubique à faces centrées, J. Phys. France. 29 (1968) 225–239, https://doi.org/10.1051/jphys:01968002902-3022500.
[26] J.F. Panzarino, Z. Pan, T.J. Rupert, Plasticity-induced restructuring of a nanocrystalline grain boundary network, Acta Mater. 120 (2016) 1–13, https://doi.org/10.1016/j.actamat.2016.08.040.
[27] Y. Mishin, D. Farkas, M.J. Mehl, D.A. Papaconstantopoulos, Interatomic potentials for monoatomic metals from experimental data and \textit{ab initio} calculations, Phys. Rev. B 59 (1999) 3393–3407, https://doi.org/10.1103/PhysRevB.59.3393.
[28] R.R. Zope, Y. Mishin, Interatomic potentials for atomistic simulations of the Ti-Al system, Phys. Rev. B 68 (2003) 024102, https://doi.org/10.1103/PhysRevB.68.024102.
[29] X.-Y. Liu, F. Ercolessi, J.B. Adams, Aluminium interatomic potential from density functional theory calculations with improved stacking fault energy, Model. Simul. Mater. Sci. Eng. 12 (2004) 665, https://doi.org/10.1088/0965-0393/12/4/007.
[30] Y. Mishin, M.J. Mehl, D.A. Papaconstantopoulos, A.F. Voter, J.D. Kress, Structural stability and lattice defects in copper: ab initio, tight-binding, and embedded-atom calculations, Phys. Rev. B 63 (2001) 224106, https://doi.org/10.1103/PhysRevB.63.224106.
[31] M.I. Mendelev, A.H. King, The interactions of self-interstitials with twin boundaries, Phil. Mag. 93 (2013) 1268–1278, https://doi.org/10.1080/14786435.2012.747012.
[32] P. Hirel, Atomsk: a tool for manipulating and converting atomic data files, Comput. Phys. Commun. 197 (2015) 212–219, https://doi.org/10.1016/j.cpc.2015.07.012.
[33] S.I. Rao, C. Varvenne, C. Woodward, T.A. Parthasarathy, D. Miracle, O.N. Senkov, W.A. Curtin, Atomistic simulations of dislocations in a model BCC multicomponent concentrated solid solution alloy, Acta Mater. 125 (2017) 311–320, https://doi.org/10.1016/j.actamat.2016.12.011.
[34] W.G. Nöhring, W.A. Curtin, Dislocation cross-slip in fcc solid solution alloys, Acta Mater. 128 (2017) 135–148, https://doi.org/10.1016/j.actamat.2017.02.027.
[35] C. Jin, Y. Xiang, G. Lu, Dislocation cross-slip mechanisms in aluminum, Phil. Mag. 91 (2011) 4109–4125, https://doi.org/10.1080/14786435.2011.602030.
[36] C. Woodward, D.R. Trinkle, L.G. Hector, D.L. Olmsted, Prediction of dislocation cores in aluminum from density functional theory, Phys. Rev. Lett. 100 (2008) 045507, https://doi.org/10.1103/PhysRevLett.100.045507.
[37] S. Plimpton, Fast parallel algorithms for short-range molecular dynamics, J. Comput. Phys. 117 (1995) 1–19, https://doi.org/10.1006/jcph.1995.1039.
[38] S. Morante, G.C. Rossi, M. Testa, The stress tensor of a molecular system: an exercise in statistical mechanics, J. Chem. Phys. 125 (2006) 034101, https://doi.org/10.1063/1.2214719.
[39] J.D. Honeycutt, H.C. Andersen, Molecular Dynamics Study of Melting and Freezing of Small Lennard-Jones Clusters, 2002. http://pubs.acs.org/doi/abs/10.1021/j100303a014. (Accessed 27 March 2017).
[40] A. Stukowski, K. Albe, Extracting dislocations and non-dislocation crystal defects from atomistic simulation data, Model. Simul. Mater. Sci. Eng. 18 (2010) 085001, https://doi.org/10.1088/0965-0393/18/8/085001.
[41] A. Stukowski, V.V. Bulatov, A. Arsenlis, Automated identification and indexing of dislocations in crystal interfaces, Model. Simul. Mater. Sci. Eng. 20 (2012) 085007, https://doi.org/10.1088/0965-0393/20/8/085007.